

Coherent excitation of the optic phonon in Si: Transiently stimulated Raman scattering with a finite-lifetime electronic excitation

D. M. Riffe and A. J. Sabbah*

Physics Department, Utah State University, Logan, Utah 84322-4415, USA

(Received 23 April 2007; published 17 August 2007)

Using 28-fs, 800-nm laser pulses we have coherently excited and subsequently probed, with time-dependent reflectivity, the Si zone-center optic phonon. The phonon-induced reflectivity change $\Delta R/R$ is well described by the response of an underdamped oscillator: $\Delta R/R \propto \exp(-t/\tau_{ph}) \cos(2\pi t/T_{ph} + \phi)$. The measured phase ϕ indicates that transiently stimulated Raman scattering (TSRS) is responsible for the coherent-phonon generation: our results are in good agreement with a recent theory of TSRS for opaque materials [T. E. Stevens *et al.*, Phys. Rev. B **65**, 144304 (2002)] when we extend the theory to include the finite lifetime of the excited charge density that couples to the oscillation. We also discuss previous experimental results on Te, Bi, Sb, Si, and Ge in light of this extended theory. Additionally, our measured period T_{ph} and decay time τ_{ph} of the Si coherent oscillation are consistent with carrier-density-dependent Raman-scattering measurements.

DOI: [10.1103/PhysRevB.76.085207](https://doi.org/10.1103/PhysRevB.76.085207)

PACS number(s): 78.47.+p, 63.20.-e, 42.65.Dr, 78.30.Am

I. INTRODUCTION

The coherent excitation of vibrational modes in a solid by ultrafast optical pulses is a sensitive probe of the coupling of electronic excitations to vibrational motion. Experiments that excite and measure coherent-phonon oscillations have been performed on a wide range of material types. Elements with *s-p* bonding (Te, Bi, and Sb) have been most widely investigated,^{1–10} while other material types that have been studied include transition metals (Zn and Cd),¹¹ cuprates (especially YBCO),^{9,12} III-VI layered compounds (GaSe and InSe),¹³ III-V semiconductors (especially GaAs),^{6,14,15} graphitic C,¹⁶ and group-IV semiconductors (Ge and Si).^{17–19} These experiments have prompted the development of a number of theories to describe the generation of the coherent oscillations in these opaque (absorbing) materials.^{2–4,13,18,20,21} Although the theories vary from semiclassical to quantum-field theoretic, each theory ultimately describes the relevant phonon mode's coherent amplitude Q as a driven harmonic oscillator,

$$\frac{d^2Q}{dt^2} + 2\beta\frac{dQ}{dt} + \Omega_0^2Q = F(t). \quad (1)$$

Here $\Omega_0/2\pi$ is the natural frequency of the (undamped) oscillator and β is the damping parameter. The differences among the theories arise in the form of the driving force $F(t)$.

Perhaps the most frequently cited theory is the semiclassical theory of Zeiger and co-workers, denoted DECP (displacive excitation of coherent phonons).² In this theory the ultrafast-laser pulse creates a time-dependent excited-carrier distribution. This distribution then couples to the vibrational mode in question, providing the force $F(t)$ in Eq. (1). The DECP theory was originally formulated to describe the excitation of modes with A_1 symmetry in *s-p* materials; for these modes the force $F(t)$ is proportional to the average value (or isotropic component) of the excited charge density. However, the theory can also describe the excitation of lower-symmetry modes, as long as the appropriate component of the excited carrier density is used as the driving force.^{8,21} The term displacive was originally included in the name of

this theory because the phase of the oscillations in the *s-p* materials for which it was developed is consistent with a displacive force. However, as we discuss in more detail below, there is nothing inherent in the DECP description that demands the force to be displacive. In fact, in the DECP theory the phase of the induced oscillations is quite sensitive to the time dependence of the coupled component of the excited charge density. In principle, then, the measured phase can be used as an experimental test of the theory.

Following the development of the DECP theory, Merlin and co-workers realized the need to also include virtual electronic excitations in the description of the force $F(t)$.^{3,4,21} Photons in the laser pulse that differ in frequency by a phonon frequency can couple to the lattice via virtual electronic excitations (as described by a Raman tensor); this Raman process provides an impulsive contribution to $F(t)$ that is proportional to the time dependence of the laser-pulse intensity. The theory that they have developed is an extension of the theory of transiently stimulated Raman scattering (TSRS) for transparent materials (where virtual transitions are the only driving mechanism for coherent oscillations^{13,21}) to opaque materials.^{3,4} The key component of the theory is a Raman tensor that places both virtual and real electronic excitations on equal footing, thus making TSRS theory applicable to both transparent and opaque materials.⁴ As in the case of DECP theory, the theory of Merlin *et al.* can be used to calculate the phase of the induced oscillations. So far, however, there have been few quantitative comparisons between the phase predicted by TSRS theory and that measured in an experiment.^{4,22}

Unfortunately, for the *s-p* materials Te, Bi, and Sb both DECP and TSRS theories predict oscillation phases for the A_1 modes that are consistent with nearly purely displacive forcing. Consequently, in these materials the phase of the oscillations has not been useful in determining which theory properly describes the generation of the coherent oscillations. Researchers have thus investigated other means to discriminate between these two theories for these materials. Citing the ratio of the coherent-oscillation amplitudes of the E_g and A_1 modes³ and the laser-frequency dependence of the A_1

mode's amplitude,⁴ Merlin and co-workers have argued that TSRS is the appropriate description. The frequency-resolved-probe time-dependent measurements of Misochko *et al.* also favor the TSRS description over the DECP theory.⁷ However, the three-pulse measurements of Lobad and Taylor have been interpreted as supporting a DECP explanation for the A_1 modes in the s - p materials.⁹

In order to investigate the extent to which the phase can be used to elucidate the excitation mechanism, we have investigated the coherent oscillation of the optic phonon in Si. Our investigation is also motivated by the fact that excitation of the optic phonon in Si (or its group-IV neighbor Ge) does not yet have a unique interpretation. In Ge the coherent oscillations were first interpreted as due to TSRS, but the cited theory was for transparent materials.¹³ The oscillations were later described by a theory where the coherent oscillations are mainly driven by the (momentum-space) anisotropic component of the excited hole distribution.^{17,18} Measurements of the same mode in Si at an excitation energy of 3.05 eV have been qualitatively discussed in terms of TSRS, but no quantitative comparison of the phase was made.¹⁹

The key result of our work is that aspects of both the DECP and TSRS theories are important in describing the excitation of the Si optic phonon. For our excitation conditions the measured phase indicates that the driving force is close to the impulsive limit. The major contribution to the impulsive nature of the force comes from virtual electronic excitations, which are an integral part of the TSRS theory. However, the finite lifetime of the coupled charge density, a feature of the DECP model (but not included in the TSRS theory), also contributes to the impulsive nature of the force. In order to unite both of these impulsive elements into the driving force, we have extended the TSRS description of Merlin and co-workers to include the finite lifetime of the coupled charge density. The phase predicted by this extended theory is in quantitative agreement with our measured phase of the Si optic phonon.

The paper proceeds as follows. In Sec. II we describe the details of our experiment. In Sec. III we quantitatively analyze our data in order to extract the phase of the coherent oscillations. We also determine the coherent-oscillation period T_{ph} and decay time τ_{ph} . In Sec. IV we derive expressions for the phase from the DECP theory, the opaque-material TSRS theory, and our extended TSRS theory. We then show that the DECP and TSRS theories predict essentially identical phases for the A_1 modes in the s - p materials, but for the T_{2g} mode in Si at our experimental conditions quite different phases are predicted, with the experimental results consistent with our extended TSRS description. We also discuss previous coherent-phonon measurements of the same phonon in Si and Ge as well as the lower symmetry E_g mode in Sb. We conclude the section with a brief discussion of the period and decay of the coherent phonon oscillations in Si and show that the results are consistent with incoherent Raman-scattering measurements. Finally, in Sec. V we summarize our results.

II. EXPERIMENTAL DETAILS

The experimental setup has been described in detail elsewhere.²³ Briefly, Gaussian-shaped 28-fs laser pulses from

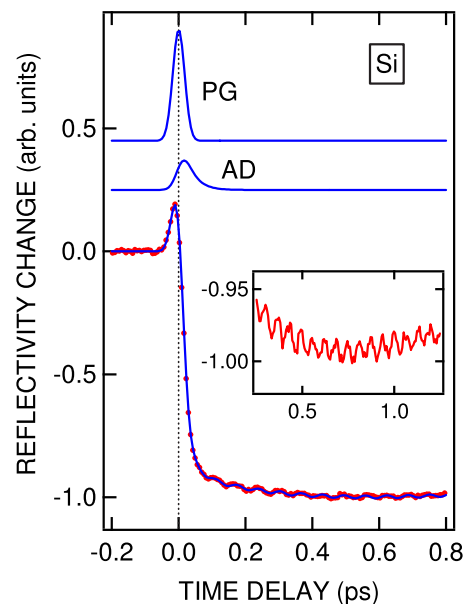


FIG. 1. (Color online) Time-dependent reflectivity change of Si from -0.2 to 0.8 ps. The points are the data and the solid line is a least-squares fit. The polarization grating (PG) and anisotropic distribution (AD) components of the fit are separately shown. The inset highlights the coherent-phonon contribution to the reflectivity change.

a 1.55-eV (800-nm) Ti:sapphire oscillator²⁴ are split into p - and s -polarized pump and probe beams, respectively. The normally incident pump excites electrons $[(5.5 \pm 0.3) \times 10^{18} \text{ cm}^{-3}]$ from the valence band (near the maximum at Γ) to the conduction band (near the six equivalent minima near the Brillouin-zone edge at X). The sample is oriented so that the pump and probe beams are polarized along (110) and $(1\bar{1}0)$, respectively, a geometry that allows for excitation and detection of the coherent oscillations.¹⁷⁻¹⁹ In these measurements the pump-probe delay time Δt ranges from -0.2 to 7.0 ps.

III. RESULTS AND ANALYSIS

A typical time-dependent reflectivity signal, which is dominated by excited-carrier induced effects, is shown in Fig. 1. After an initial positive transient, the reflectivity decreases quite rapidly (until $\Delta t \approx 80$ fs) and then more slowly (up to $\Delta t \approx 700$ fs). It then slowly increases and recovers to the initial baseline in ~ 1 ns.²⁵ The coherent oscillation of the Si zone-center phonon, shown more clearly in the inset of Fig. 1, is manifest as small, periodic variations that are apparent after the rapid decrease in reflectivity.

The carrier-induced variations in reflectivity, which have been delineated in detail elsewhere,²³ are relevant to our analysis of the coherent-phonon excitation. Briefly, the carrier-induced variations comprise features due to the anisotropic (in k space) component of the carrier distribution as well as variations due to the isotropic component of the distribution.²⁶ The anisotropic part of the distribution contributes two features, a polarization-grating (PG) peak that

arises from the pump pulse scattering from the polarization grating formed by the orthogonally polarized pump and probe beams and an anisotropic-distribution (AD) peak that arises from the probe pulse interacting with the anisotropic carrier distribution produced by the pump.²⁷ The PG peak is purely a correlation of the pump and probe beams at the sample and so allows precise (± 0.3 fs) determination of $\Delta t = 0$ in the experiment. This is essential for accurate determination of the phase of the coherent-phonon oscillations. The AD peak is important because its shape is determined in part by the decay time τ_C of the anisotropic component of the carrier distribution, which is the component that couples to the optic phonon in Si.¹⁸ The PG and AD peaks are responsible for the initial peak in the reflectivity observed in Fig. 1. The isotropic component of the carrier distribution is responsible for the remainder (large overall drop and slow recovery) of the reflectivity changes.^{23,25}

In order to determine the phase ϕ of the oscillations²⁸ we fit the reflectivity variations shown in Fig. 1 with a model that includes all of the carrier-induced variations²³ in addition to a function that describes the reflectivity change produced by the coherent-phonon oscillations. For the oscillations we assume that the phonon-induced reflectivity changes are proportional to the coherent-phonon displacement and use the response of a transiently excited oscillator to write

$$\frac{\Delta R_{ph}}{R}(\Delta t) = A_F(\Delta t) \frac{\Delta R_{ph}^{\max}}{R} \exp\left(-\frac{\Delta t}{\tau_{ph}}\right) \cos\left(\frac{2\pi\Delta t}{T_{ph}} + \phi\right). \quad (2)$$

The fitting parameters are the amplitude $\Delta R_{ph}^{\max}/R$, phonon coherence time $\tau_{ph} = 1/\beta$, period of oscillation $T_{ph} = 2\pi/\Omega_1$ (where $\Omega_1 = \sqrt{\Omega_0^2 - \beta^2}$), phase ϕ , and the zero-time delay (which is implicit in Δt). The function $A_F(\Delta t)$ describes the initial transient response of the oscillator. Generally, $A_F(\Delta t)$ equals zero before the driving force starts, equals 1 after the driving force is over, and has a shape that depends upon the time dependence of the force (and parameters of the oscillator). We have fit the data with a variety of approximations for $A_F(\Delta t)$. However, because the amplitude $\Delta R_{ph}^{\max}/R$ of the phonon oscillations is much smaller than the amplitudes of any of the carrier-induced contributions to the reflectivity, the exact form of $A_F(\Delta t)$ does not significantly impact the result for the phase ϕ .

The results of the fitting are shown as the solid line through the data points in Fig. 1. The AD and PG parts of the carrier-induced response are individually shown, vertically displaced for clarity. As mentioned above, the maximum of the PG peak defines the zero-time delay (as indicated by the vertical dotted line). The residuals of the fit are statistical in nature,²³ indicating that the model provides an excellent description of the data. From the analysis we determine the phase to be $\phi = 88^\circ \pm 14^\circ$. Relevant to the discussion below concerning the coherent-phonon-generation mechanism, from the AD peak we also obtain the anisotropic-distribution decay time $\tau_C = 32 \pm 5$ fs.²³

The period T_{ph} and decay time τ_{ph} are also fitting parameters in the above analysis. However, their values are obtained with more consistency among the data sets via a sim-

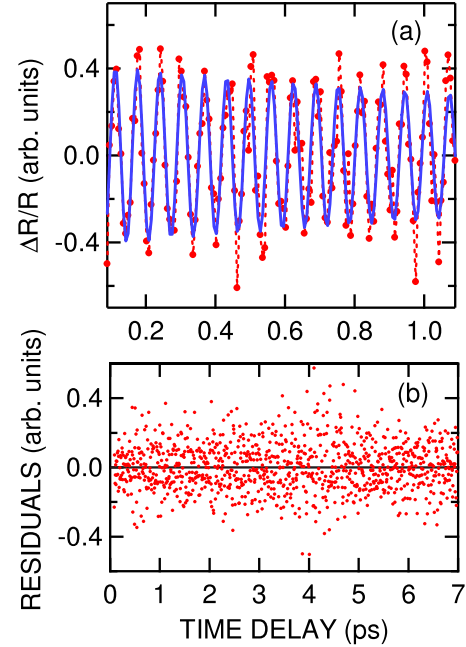


FIG. 2. (Color online) Coherent-phonon contribution to the reflectivity change of Si over a 1.0-ps time scale. (a) The points are the data and the solid line is a least-squares fit. (b) Residuals of the fit to the coherent phonon oscillations over a 7-ps time scale.

pler analysis in which the carrier-induced variations in the reflectivity are removed before the least-squares fitting. The carrier-induced variations are removed by (i) only using data after the large drop in reflectivity (after $\Delta t \approx 80$ fs) and (ii) high-pass filtering the data.²⁹ The filtered data are then fit by simply using Eq. (2) with $A_F(\Delta t)$ set equal to 1:

$$\frac{\Delta R_{ph}}{R}(\Delta t) = \frac{\Delta R_{ph}^{\max}}{R} \exp\left(-\frac{\Delta t}{\tau_{ph}}\right) \cos\left(\frac{2\pi\Delta t}{T_{ph}} + \phi\right). \quad (3)$$

A typical fit and the residuals are illustrated in Fig. 2.³⁰ A visual comparison of the filtered data and the fit are shown in Fig. 2(a). That Eq. (3) accurately models the filtered data over the full 7-ps delay time is evident in the statistical nature of the residuals, which are plotted in Fig. 2(b). From this analysis we obtain $T_{ph} = 64.07 \pm 0.07$ fs and $\tau_{ph} = 2.80 \pm 0.15$ ps.

We have also analyzed the data in frequency space to obtain values of T_{ph} and τ_{ph} . Figure 3 shows the Fourier transform of one data set and its corresponding fit, where the fitting function is the Fourier transform of Eq. (3) (windowed with a 7-ps window).³¹ From this frequency-based analysis we obtain results consistent with the time-based analysis: $T_{ph} = 64.16 \pm 0.05$ fs and $\tau_{ph} = 2.82 \pm 0.40$ ps.

IV. DISCUSSION

A. Theoretically predicted phases

Here we discuss the phase of the coherent oscillations predicted by the DECP model, the TSRS model, and an extension of the TSRS model that includes the finite lifetime of the coupled carrier distribution. For each of these models the

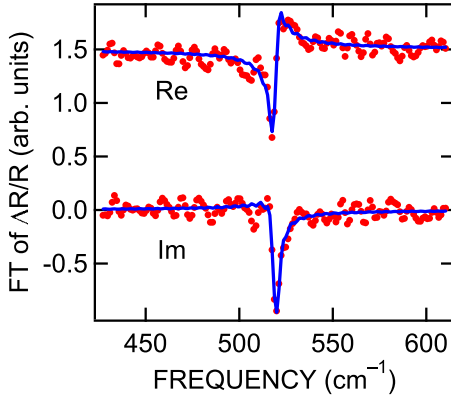


FIG. 3. (Color online) Fourier transform (FT) of the coherent-phonon contribution to the reflectivity changes. The points are the data and the solid line is a least-squares fit. For clarity, the Re part of the FT has been vertically displaced 1.5 units.

phase is calculated using the general formula

$$\phi = \arctan \left\{ \frac{\text{Im} \left[i\hat{F}(-\Omega_1 - i\beta) \right]}{\text{Re} \left[i\hat{F}(-\Omega_1 - i\beta) \right]} \right\}, \quad (4)$$

which is derived in Appendix A. Here $\hat{F}(\Omega)$ is the Fourier transform of the driving force $F(t)$.

1. DECP model

In the DECP model the force $F(t)$ is assumed to be proportional to the density n_C of the coupled component of the excited charge density. That is, the model assumes $F(t) = bn_C(t)$, where b is the proportionality constant. In the s - p metals the isotropic component of the charge density couples to the A_1 modes.² Pertinent to the case at hand, the anisotropic component of the excited carrier distribution couples to the optic phonon in Si, which has T_{2g} symmetry.^{17,18,21} In modeling the dynamics of $n_C(t)$ it is assumed that the carriers are linearly excited by the laser pulse intensity $I(t)$ and the decay of $n_C(t)$ is treated in the relaxation-time approximation with a constant relaxation time τ_C . With these approximations $n_C(t)$ is governed by

$$\frac{dn_C}{dt} + \gamma n_C = aI(t), \quad (5)$$

where $\gamma = 1/\tau_C$ and a is a constant that is determined by the optical response of the material. With the initial condition $n_C(t \rightarrow -\infty) = 0$ Eq. (5) can be solved and the force expressed as

$$F(t) = ab \exp(-\gamma t) \int_{-\infty}^t dt' I(t') \exp(\gamma t'). \quad (6)$$

The Fourier transform of Eq. (6) can be written as

$$\hat{F}(\Omega) = \frac{ab}{\gamma - i\Omega} \hat{I}(\Omega). \quad (7)$$

Thus

$$i\hat{F}(-\Omega_1 - i\beta) = ab \frac{[\Omega_1 + i(\gamma - \beta)]}{\Omega_1^2 + (\gamma - \beta)^2} \hat{I}(-\Omega_1 - i\beta). \quad (8)$$

Equation (8) can be significantly simplified by noting that $\beta \ll \Omega_1$ for most coherent oscillations of interest. Further, for a symmetric laser pulse $\hat{I}(-\Omega_1) = \hat{I}(\Omega_1)$. Thus in Eq. (8) we may replace $\hat{I}(-\Omega_1 - i\beta)$ by $\hat{I}(\Omega_1)$ with very little error in the calculated phase. The error that results from this approximation is of order $\Omega_1 \beta \tau_p^2$, which is generally negligible. (This is because $\beta \ll \Omega_1$ and coherent oscillations are only generated for $\Omega_1 \tau_p \lesssim 1$. For example, using parameters appropriate to our experiment, this approximation results in an error in ϕ of only 0.3° .) Thus we may write

$$i\hat{F}(-\Omega_1 - i\beta) = ab \frac{[\Omega_1 + i(\gamma - \beta)]}{\Omega_1^2 + (\gamma - \beta)^2} \hat{I}(\Omega_1). \quad (9)$$

Using the fact that $\hat{I}(\Omega_1)$ is real for a symmetric pulse, the substitution of Eq. (9) into Eq. (4) yields the theoretical DECP phase

$$\phi_{DECP} = \arctan \left(\frac{\gamma - \beta}{\Omega_1} \right). \quad (10)$$

The dispersive and impulsive limits of the DECP model are readily deduced from Eq. (10). The dispersive limit ($\phi \approx 0$), which is observed for the A_1 modes in s - p materials, occurs when $\gamma \ll \Omega_1$ —that is, when the coupled charge-density decay time is much longer than the period of the coherent oscillation. Conversely, the impulsive limit ($\phi \approx \pi/2$) occurs when the charge-density decay constant γ is large compared to the oscillation frequency Ω_1 .

2. TSRS model

As mentioned in the Introduction, the opaque-material TSRS theory puts virtual excitations on equal footing with the real transitions that are described by the DECP theory. Useful for our purposes here, from their TSRS theory Merlin and co-workers have derived an approximate expression for $\hat{F}(\Omega)$ that can be expressed in our notation as

$$\hat{F}(\Omega) = C \left(\varepsilon'_1 + \frac{2\varepsilon_2}{-i\Omega} \right) \hat{I}(\Omega), \quad (11)$$

where C is a constant, $\hat{\varepsilon} = \varepsilon_1 + i\varepsilon_2$ is the dielectric function of the material, and $\varepsilon'_1 = d\varepsilon_1/d\omega$.⁴ Both ε'_1 and ε_2 are evaluated at the center frequency ω_0 of the laser pulse. The first term ($\propto \varepsilon'_1$) is the contribution from virtual excitations, while the second term ($\propto \varepsilon_2$) is the (absorption) contribution from the coupled charge density. Equation (11) was derived under the assumptions that (i) the dielectric function is dominated by direct electronic transitions, (ii) two-band processes dominate the Raman tensor, and (iii) the excited charge density has an infinite lifetime ($\gamma = 0$).^{3,4} Because $\gamma = 0$ in this model, the excited charge density contributes a dispersive force only. (Notice that $[2C\varepsilon_2/(-i\Omega_1)]\hat{I}(\Omega)$ is equivalent to $\hat{F}(\Omega)$ in the DECP model [Eq. (7)] with $\gamma = 0$.) From Eq. (11) and again using the same approximation for $\hat{I}(-\Omega_1 - i\beta)$, we obtain from the TSRS model

$$i\hat{F}(-\Omega_1 - i\beta) = C \frac{\Omega_1 2\varepsilon_2 + i[(\Omega_1^2 + \beta^2)\varepsilon'_1 - \beta 2\varepsilon_2]}{\Omega_1^2 + \beta^2} \hat{I}(\Omega_1). \quad (12)$$

Thus the phase within the TSRS description is given by

$$\phi_{TSRS} = \arctan \left[\frac{(\Omega_1^2 + \beta^2)\varepsilon'_1}{\Omega_1 2\varepsilon_2} - \frac{\beta}{\Omega_1} \right]. \quad (13)$$

Generally, we can ignore β^2 compared to Ω_1^2 , and so this simplifies to

$$\phi_{TSRS} = \arctan \left(\frac{\Omega_1 \varepsilon'_1}{2\varepsilon_2} - \frac{\beta}{\Omega_1} \right). \quad (14)$$

We could also neglect the β/Ω_1 term in Eq. (14). However, by keeping it we clearly see that if virtual transitions are insignificant, then, as expected, ϕ_{TSRS} reduces to the $\gamma=0$ ϕ_{DECP} result. This, again, is the dispersive limit $\phi \approx 0$. In the TSRS model the driving force can also be impulsive, but instead of being due to the finite lifetime of the coupled charge density, the impulsive component arises from the virtual transitions. Indeed, Eq. (14) shows that in the TSRS model the impulsive limit occurs for $2\varepsilon_2 \ll \Omega_1 \varepsilon'_1$.

3. TSRS model with $\gamma \neq 0$

As evident in the discussion above, each of these two models of coherent excitation has its own limitation: the DECP model does not include virtual transitions, while the TSRS model neglects the finite lifetime of the coupled charge density. For the widely studied A_1 modes in the s - p materials, neither limitation is very important: the coupled charge density typically decays quite slowly, and virtual transitions are relatively unimportant. Thus both models are essentially equivalent and quite correctly predict dispersive excitation of the A_1 modes. However, for the case at hand of the Si optic phonon, the coupled charge density decays on a time scale that is shorter than the period of oscillation. Further, as we show below, virtual transitions are also important in the coherent excitation process. We thus require a theory that includes both virtual and real transitions as well as a finite decay constant γ .

In Appendix B we extend the two-band TSRS result [Eq. (11)] to nonzero values of γ , from which we now obtain the phase. The key result of this appendix is

$$\hat{F}(\Omega) = C \frac{\Omega}{\Omega + i\gamma} \left(\varepsilon'_1 + \frac{2\varepsilon_2}{-i\Omega} \right) \hat{I}(\Omega). \quad (15)$$

With the same approximation for $\hat{I}(\Omega_1)$ as above we obtain from Eq. (15)

$$i\hat{F}(-\Omega_1 - i\beta) = C \frac{\Omega_1(2\varepsilon_2 - \gamma\varepsilon'_1) + i[(\Omega_1^2 + \beta^2 - \gamma\beta)\varepsilon'_1 + (\gamma - \beta)2\varepsilon_2]}{\Omega_1^2 + (\gamma - \beta)^2} \hat{I}(\Omega_1). \quad (16)$$

Noting again that $\beta^2 \ll \Omega_1^2$ and that typically $\gamma\beta \ll \Omega_1^2$, we can express the phase as

$$\phi_{RSFL} = \arctan \left[\frac{\Omega_1^2 \varepsilon'_1 + (\gamma - \beta)2\varepsilon_2}{\Omega_1(2\varepsilon_2 - \gamma\varepsilon'_1)} \right]. \quad (17)$$

(Here *RSFL* stands for *Raman scattering finite lifetime* to indicate that γ is not necessarily zero.) In the appropriate limit, either $\varepsilon'_1=0$ or $\gamma=0$, Eq. (17) simplifies to either the DECP or TSRS result, respectively.

4. Summary of the theoretical phases

By defining three dimensionless quantities $\bar{\beta} = \beta/\Omega_1$, $\bar{\gamma} = \gamma/\Omega_1$, and $\bar{\varepsilon} = \Omega_1 \varepsilon'_1 / 2\varepsilon_2$, the results for the three phases [Eqs. (10), (14), and (17)] can be succinctly expressed as

$$\phi_{DECP} = \arctan(\bar{\gamma} - \bar{\beta}), \quad (18)$$

$$\phi_{TSRS} = \arctan(\bar{\varepsilon} - \bar{\beta}), \quad (19)$$

and

$$\phi_{RSFL} = \arctan \left(\frac{\bar{\varepsilon} + \bar{\gamma} - \bar{\beta}}{1 - \bar{\varepsilon}\bar{\gamma}} \right). \quad (20)$$

We further note that if $\bar{\beta}$ is negligible compared to $\bar{\gamma}$ and $\bar{\varepsilon}$, then the relationship

$$\phi_{RSFL} = \phi_{TSRS} + \phi_{DECP} \quad (21)$$

holds. That is, the contributions to the phase from virtual transitions and the finite lifetime of the coupled carriers are independent of one another and simply additive.

Figure 4 shows a contour plot of ϕ_{RSFL} as a function of $\bar{\gamma}$ and $\bar{\varepsilon}$ (under the condition that $\bar{\beta}$ is negligible). The DECP result for the phase occurs along the horizontal ($\bar{\varepsilon}=0$) axis while the TSRS result is found along the vertical ($\bar{\gamma}=0$) axis. Note that generally $\bar{\gamma} > 0$ but $\bar{\varepsilon}$ can have either sign. Along either of these two axes the dispersive limit ($\phi=0$) occurs at the origin and the impulsive limit ($\phi=90^\circ$) is approached for large values of either $\bar{\gamma}$ or $\bar{\varepsilon}$ (whichever is appropriate). However, the impulsive limit can also occur for combinations of modest values of both quantities. Also note that the dispersive limit occurs along the line defined by $\bar{\varepsilon} = -\bar{\gamma}$, corresponding to $\phi_{TSRS} = -\phi_{DECP}$.

B. Comparison of experimental and theoretical phases

We now compare our experimental phase from Si and previous experimental phases from a variety of materials—Te, Bi, Sb, Si, and Ge—with the phases predicted by these three theoretical models. We first consider the A_1 modes in the s - p materials and demonstrate why the phases are all very close to the dispersive limit $\phi=0$. We then discuss lower symmetry modes in Sb, Si, and Ge.

Table I summarizes the pertinent experimental and theoretical quantities. Concomitant experimental values of Ω_1 , $\hbar\omega_0$, γ , β , and ϕ_{expt} all come from the same study.^{2,3,5,10,17,19} We have determined ε'_1 and ε_2 from measured optical constants.³²⁻³⁶ Values of the normalized parameters $\bar{\varepsilon}$, $\bar{\gamma}$, and $\bar{\beta}$ are also indicated. These values are used to calculate the

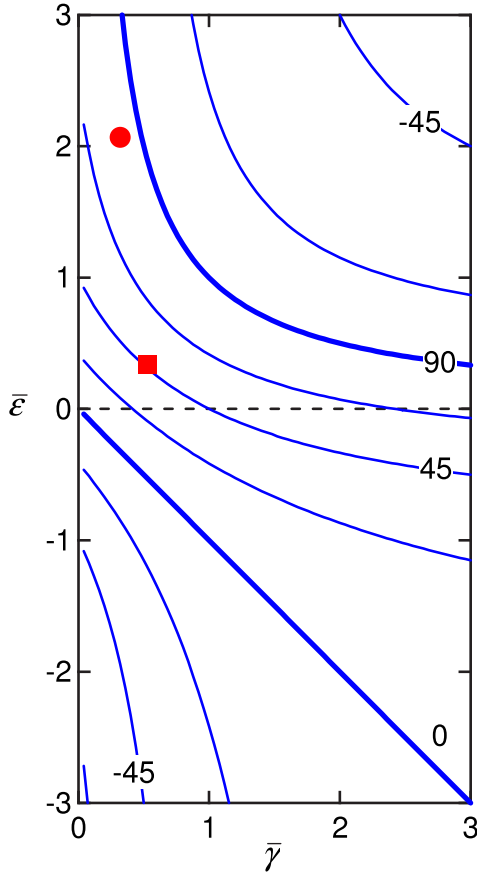


FIG. 4. (Color online) Contours of ϕ_{RSFL} as a function of $\bar{\gamma}$ and $\bar{\epsilon}$. Also plotted are values of ϕ_{RSFL} for Si at photon energies of 1.55 eV (solid circle) and 3.05 eV (solid square).

tabulated values of the theoretical phases ϕ_{DECP} , ϕ_{TSRS} , and ϕ_{RSFL} .

For the A_1 modes in Te, Bi, and Sb the values of $\bar{\epsilon}$, $\bar{\gamma}$, and $\bar{\beta}$ are all much less than 1, resulting in calculated phases very close to the displacive limit $\phi=0$. In these materials the displacive limit is the result of both strong absorption, which results in a small value of $\bar{\epsilon}$, and a relatively long lifetime of the coupled charge density, which results in a small value of $\bar{\gamma}$. In four of the six cases there is excellent agreement with the experimentally determined phase ϕ_{expt} ; the two minor exceptions are Bi at 1.55 eV and Sb at 1.52 eV. The fact that the Raman-scattering cross section of Bi is well described by the two-band model for photon energies between 1.55 and 2.7 eV (Ref. 34) suggests that there may be a slight systematic error in the reported value of ϕ_{expt} . In the case of Sb, however, the simple connection of the two-band model to the dielectric function is not valid for photon energies below 1.9 eV.³⁴ Thus the theory for Sb at 1.55 eV should only be taken as qualitative. However, even with the inclusion of these two exceptions, the phases of the A_1 modes in the s - p materials are all reasonably consistent with the displacive limit $\phi=0$, which we interpret as due to a combination of strong absorption and slow decay of the coupled charge density.

One way to get away from the displacive limit is to investigate modes with lower symmetry, such as those in the last four entries of Table I. These lower-symmetry modes couple to lower-symmetry components of the charge density, which typically decay on a time scale shorter than the oscillation period. For example, in Si for our experimental conditions the anisotropic charge-density component that couples to the T_{2g} mode decays with a time constant $\tau_C = 32 \pm 5$ fs, resulting in $\bar{\gamma} = 0.32$, which is significantly larger than $\bar{\gamma}$ for any of the A_1 modes discussed above. Similarly, a much shorter τ_C is observed for the E_g mode in Sb: the

TABLE I. Experimental and theoretical phases (and associated parameters) for Te, Bi, Sb, Si, and Ge.

Mode	Ω_1 (THz)	$\hbar\omega_0$ (eV)	ϵ'_1 (10^{-14} s)	ϵ_2	γ (THz)	β (THz)	$\bar{\epsilon}$ (10^{-2})	$\bar{\gamma}$ (10^{-2})	$\bar{\beta}$ (10^{-2})	ϕ_{DECP} (deg)	ϕ_{TSRS} (deg)	ϕ_{RSFL} (deg)	ϕ_{expt} (deg)
Te A_1	22.6 ^a	1.98	-4.5 ^b	33	1.59	0.79	-1.5	7.0	3.5	2	-3	1	7 ± 9
	21.1 ^c	1.50	0.53 ^b	12	1.33	0.50	0.61	6.0	2.2	2	-1	2	0
Bi A_{1g}	18.2 ^a	1.98	0.63 ^d	10	0.10	0.41	0.58	0.53	2.3	-1	-1	-1	-13 ± 13
	18.4 ^e	1.55	0.53 ^d	19	0.31	0.26	0.26	1.7	1.4	0	-1	0	15 ± 1
Sb A_{1g}	28.3 ^a	1.98	-0.63 ^f	25	0.60	0.34	-0.35	2.1	1.2	1	-1	0	3 ± 4
	28.3 ^g	1.52	-0.52 ^f	37	0.50	0.27	-0.20	1.8	0.96	0	-1	0	-23 ± 11
Sb E_g	21.4 ^g	1.52	-0.52 ^f	37	>10	0.56	-0.15	>50	2.6	>24	-2	>24	43 ± 8
Si T_{2g}	98.1 ^h	1.55	0.20 ⁱ	0.047	32	0.36	210	32	0.36	18	64	82	88 ± 14
	95.8 ^j	3.05	2.4 ⁱ	3.4	51	0.77	34	53	0.80	28	19	47	23
Ge T_{2g}	57.1 ^k	2.00	1.3 ⁱ	11		0.37	3.3		0.65		2		

^aReference 2.

^bReference 32.

^cReference 10.

^dReferences 33 and 34.

^eReference 5.

^fReference 35.

^gReference 3.

^hThis study.

ⁱReference 36.

^jReference 19.

^kReference 17.

reflectivity data in Fig. 1(a) of Ref. 3 show that the electronic decay time τ_C associated with the E_g mode is at least as short as ~ 100 fs (which is approximately the time resolution of that experiment). This is much faster than $\tau_C \approx 2$ ps associated with the A_1 mode (which is also evident in the same figure).

This significantly shorter τ_C for the Sb E_g vibration provides, within the context of our extended TSRS theory, a natural explanation of the (nondisplacive) experimental phase $\phi_{\text{expt}} = 43 \pm 8$ degrees. As indicated in Table I, an upper bound of 100 fs on τ_C (corresponding to $\bar{\gamma} \geq 0.5$) implies a finite-lifetime contribution to the phase of at least 24° . Conversely, if we start with the experimental phase of 43° , we can infer a value $\bar{\gamma} \approx 1$, which corresponds to $\tau_C \approx 50$ fs. Without such a significant difference in the decay times of the charge densities that couple to the A_1 and E_g modes, we would expect both modes to have essentially the same phase, a result that is clearly inconsistent with experiment.³

For the T_{2g} optic phonon in Si a small value of τ_C also contributes to a nonzero theoretical phase. In addition, because the absorption is relatively weak, virtual transitions also provide a contribution to the phase. For our experimental conditions we calculate $\phi_{RSFL} = 82^\circ$, in excellent agreement with our experimental result $\phi_{\text{expt}} = 88^\circ \pm 14^\circ$. For this mode $\bar{\beta}$ is much less than both $\bar{\gamma}$ and $\bar{\epsilon}$, so that Eq. (21) holds. We can thus unambiguously assign most of the impulsive character to virtual excitations with a smaller contribution from the finite lifetime of the coupled charge density. This is illustrated in Fig. 4, which plots ϕ_{RSFL} for Si vs $\bar{\gamma}$ and $\bar{\epsilon}$ (as the solid circle).

We should point out that this precise quantitative agreement between ϕ_{RSFL} and ϕ_{expt} for Si is actually slightly surprising. That the theoretical phases ϕ_{TSRS} and ϕ_{RSFL} can be simply related to the dielectric function is partly based on the near equivalence of the sums that appear in the quantum descriptions of the Raman tensor^{3,4} and the dielectric function,³⁷ both of which involve only direct electronic transitions.^{38–40} In the photon-energy range of our laser (1.55 eV), ϵ_1 is indeed dominated by direct transitions (which occur at higher frequencies).³⁶ However, ϵ_2 is thought to be due primarily to indirect transitions (as described in Sec. II above); the contribution of direct transitions to ϵ_2 is believed to be negligible. Thus, the value of ϕ_{TSRS} calculated using Eq. (14) is likely an underestimate. However, even the extreme impulsive-limit value of $\phi_{TSRS} = 90^\circ$ would imply $\phi_{RSFL} = 108^\circ$, which is still in reasonable agreement with our experimental result. Thus, even with this uncertainty in the size of ϕ_{TSRS} , it is clear that virtual excitations are the major contributor to the nonzero phase of the Si optic-phonon oscillation.

Coherent excitation of the Si T_{2g} optic phonon has been previously measured with 3.05 eV photons by Hase *et al.*; an experimental phase of 23° was reported.¹⁹ In order to compare our theory with this result it has been necessary to determine γ from the data of Hase *et al.* We have done this by fitting the decay of $\Delta R/R$ in Fig. 1(b) of Ref. 19, which was taken using the electro-optic sampling geometry with the phonon oscillation suppressed and is thus solely a combination of PG and AD signals. As shown in Fig 5(a), $\Delta R/R$

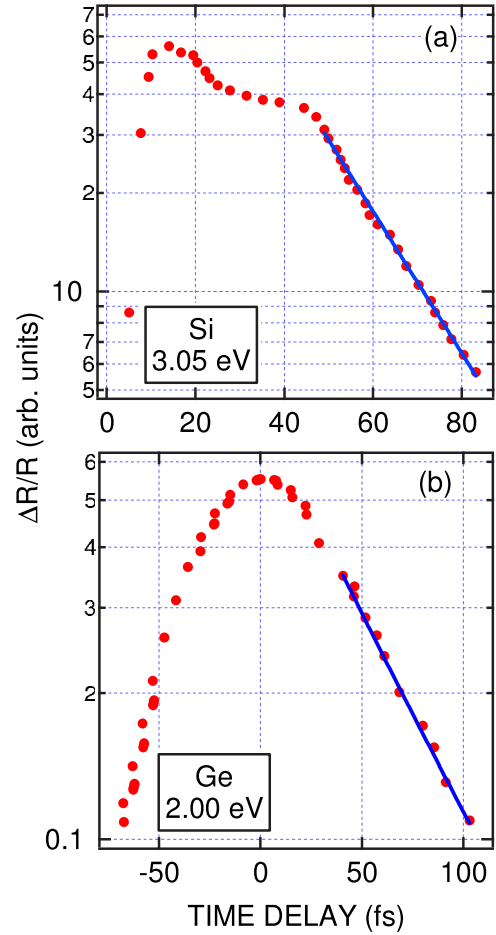


FIG. 5. (Color online) Reflectivity changes measured with the electro-optic sampling geometry from (a) Si at 3.05 eV from Ref. 19 and (b) Ge at 2.00 eV from Ref. 18. The points are the data and the solid lines are exponential-decay fits to the tails of the data.

shows an exponential decay for delay times ≥ 50 fs. From the fit to this part of the data [shown as the straight line in Fig. 5(a)] we have determined a value of $\tau_C = 19$ fs, corresponding to $\gamma = 51$ THz. With this parameter we calculate $\phi_{RSFL} = 47^\circ$, with individual contributions of 28° and 19° from the finite decay time and virtual transitions, respectively. Although no estimate of experimental uncertainty in the phase was provided,¹⁹ the lack of quantitative agreement in this case is somewhat unexpected. This is because conditions are ideal for comparison with the theoretical models: for Si excited with 3.05 eV photons (which is just below the E_1 and $E_1 + \Delta_1$ gaps) the dielectric function $\hat{\epsilon}$ is dominated by direct absorption and the Raman scattering tensor is effectively a two-band tensor (from at least 1.8 eV up to 3.8 eV).^{41,42} Nonetheless, because ϕ_{DECP} is roughly the same at 1.55 and 3.05 eV excitation, we can attribute the significantly smaller phase at 3.05 eV to a reduction in the contribution from virtual transitions, as evidenced by the significant differences in $\bar{\epsilon}$ (and thus ϕ_{TSRS}) for these two cases. This last point is emphasized in Fig. 4, where we also plot ϕ_{RSFL} at 3.05 eV (as the solid square). We also compare the difference in phase between our measurement and that of Hase *et al.* in Fig. 6, where we plot ϕ_{RSFL} versus photon

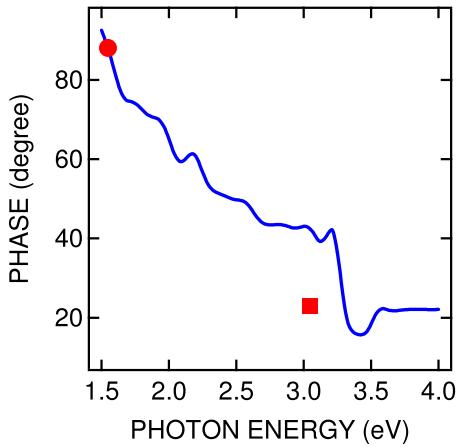


FIG. 6. (Color online) The coherent-phonon phase of Si vs photon energy. The solid line is ϕ_{RSFL} assuming a constant contribution from ϕ_{DECP} of 23° . The solid circle and solid square are experimental results from this study and Ref. 19, respectively.

energy, assuming a constant contribution of 23° (the average of the 1.55 and 3.05 eV values) from ϕ_{DECP} . The theoretical curve shows a nearly monotonic decrease in phase as the photon energy is increased. As evident from Fig. 6, measurements of the Si coherent phonon at other frequencies in this range would provide an ideal test of the current model.

The last entry in Table I is for Ge excited by 2.0-eV photons. For this excitation energy Scholz *et al.* have identified the anisotropic component of the excited hole distribution as the main driver of the coherent excitation.¹⁸ Our calculated value of $\phi_{TSRS}=2^\circ$ confirms their assessment: virtual transitions are not important in excitation of the Ge optic phonon. However, a more detailed comparison of their experiment with our theory requires a bit more analysis. This is because Scholz *et al.* reference their experimental phase (which is $\sim 90^\circ$) to the peak of the electronic contribution to the reflectivity change. However, due to the AD component of this response, this peak is not coincident with the true (pump-probe) zero-time delay.

We can estimate the shift of the peak in electronic response using our models of the PG and AD response functions.²³ However, there are two parameters needed for the calculation that have significant uncertainties: (i) the ratio of the amplitudes of the PG and AD responses and (ii) the value of τ_C . We have fit the data of Fig. 1 of Ref. 18 in an attempt to determine the relative contributions of the PG and AD responses. While the AD response appears to dominate the PG response, the data do not lend themselves to a unique analysis—relatively good fits are obtained with both positive and negative PG peaks; therefore, in the following analysis we have assumed that the PG contribution is simply zero. As for τ_C , Scholz *et al.* have argued, based on experimental results from GaAs,⁴³ that $\tau_C \leq 8$ fs for their experiment on Ge. On the other hand, their data suggest that τ_C may be much longer. In Fig. 5(b) we plot the time-integrated data from Fig. 1 of Ref. 18. As evident in the figure, between ~ 50 and 100 fs the data show an exponential decay; our fit to this portion of the data yields a decay constant of ~ 50 fs. We thus take this value as an upper bound on τ_C .

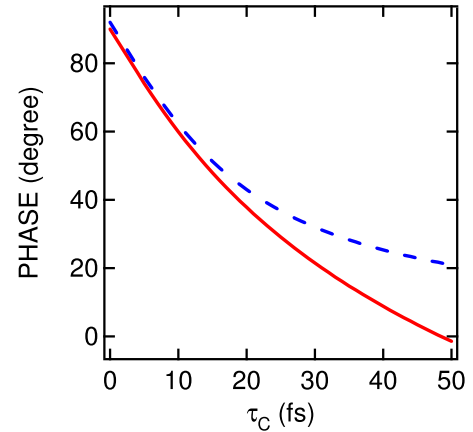


FIG. 7. (Color online) Phase of Ge vs coupled charge-density decay time τ_C . The solid line is the corrected experimental phase of Ref. 18. The dashed line is ϕ_{RSFL} .

We have therefore calculated the time delay of the electronic-response peak as a function of τ_C from 0 to 50 fs. Using this delay we have converted the reported phase of 90° to a “corrected” experimental phase consistent with the other phases in Table I. The results are shown as the solid line in Fig. 7. In the limit $\tau_C \rightarrow 0$, the peak of the electronic response approaches a delay of zero fs, and thus the correction to the reported value approaches zero degrees. However, as τ_C increases, the peak in the electronic response becomes increasingly delayed. For $\tau_C=50$ fs, the delay is 28 fs, equivalent to correction of -91.5° , which results in a corrected phase of -1.5° . For comparison with this corrected experimental phase we also plot ϕ_{RSFL} (which depends upon τ_C through $\bar{\gamma}$) as the dashed line in Fig. 7. For small values of τ_C , the experimental and theoretical values show excellent agreement, but even for $\tau_C=50$ fs, the difference is only $\sim 20^\circ$. We can thus conclude that the experimental observation of Scholz *et al.* is not inconsistent with our RSFL model, irrespective of the exact value of τ_C .

C. Coherent-phonon period and decay time

Incoherent Raman scattering has been extensively used to study the Si optic phonon.^{44–54} The intrinsic material exhibits a Lorentzian peak with a center frequency $\bar{\nu}$ close to 520 cm^{-1} and a room-temperature natural width [full width at half maximum (FWHM)] $\bar{\Gamma}$ slightly less than 3 cm^{-1} .⁵⁵ The intrinsic width is due to the finite lifetime of the optic phonon, which anharmonically decays into two or more acoustic phonons.^{46,55,56} Raman studies on heavily doped *p*-type samples show that with increasing doping the Lorentzian peak evolves into a Fano line shape, indicative of coupling to an excitation continuum, which in this case consists of hole excitations between valence bands.^{49,50,52,57} The extra decay channel provided by this coupling results in an increasing natural width with increasing hole concentration.^{47,50,52,53} Additionally, the center frequency shifts downwards as the hole concentration increases.^{47,50,52,53}

The increase in natural width has been observed for hole densities as low as $5 \times 10^{18} \text{ cm}^{-3}$, which is comparable to

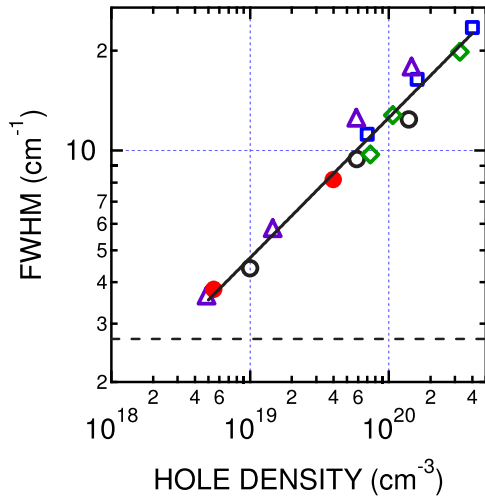


FIG. 8. (Color online) Linewidth of the Si optic-phonon Raman peak vs hole density. The open symbols are from Raman scattering measurements: circles, Ref. 47; squares, Ref. 50; triangles, Ref. 53; diamonds, Ref. 52. The two solid symbols are the equivalent widths deduced from the optic-phonon decay time τ_{ph} in this work ($5.5 \times 10^{18} \text{ cm}^{-3}$) and Ref. 19 ($4 \times 10^{19} \text{ cm}^{-3}$). The solid line is a power-law fit to the Raman scattering results. The dashed line indicates the low-density limit (2.7 cm^{-1}) of the line width (Ref. 55).

our excited carrier density of $5.5 \times 10^{18} \text{ cm}^{-3}$.⁵³ In Fig. 8 we plot Raman-scattering-determined values of the natural width as a function of hole density,^{47,50,52,53} which show a power-law increase in the width from 3.5 cm^{-1} at $5 \times 10^{18} \text{ cm}^{-3}$ to 23 cm^{-1} at $4 \times 10^{20} \text{ cm}^{-3}$. The decay time τ_{ph} measured in our experiment converts to an equivalent Lorentzian (or Fano) natural width via $\bar{\Gamma} = 1/(\pi c \tau_{ph})$, where c is the speed of light. Our time-domain-analyzed result of $\tau_{ph} = 2.80 \pm 0.15 \text{ ps}$ thus corresponds to a natural width of $3.8 \pm 0.3 \text{ cm}^{-1}$. This ultrafast inferred width and a similarly inferred width at higher excitation density from a previous ultrafast measurement¹⁹ are also plotted in Fig. 8. As shown there these two ultrafast measurements are consistent with widths from the incoherent Raman scattering measurements. This is not surprising: in Si, the laser excited carriers thermalize with the lattice on a time scale of $\sim 250 \text{ fs}$;²³ thus, in both the incoherent Raman and coherent ultrafast measurements the optic phonon interacts with a thermalized room-temperature hole distribution.

The coupling to the hole continuum also produces a shift in the center frequency. However, the shift in center frequency is not significant for hole densities $\leq 5 \times 10^{19} \text{ cm}^{-3}$,⁵³ which is substantially greater than our carrier concentration of $5.5 \times 10^{18} \text{ cm}^{-3}$. Reported values of $\bar{\nu}$ from Raman studies for $p < 5 \times 10^{19} \text{ cm}^{-3}$ (which include an estimation of the uncertainty) are 523 ± 1 ,⁴⁴ $520.2 \pm 0.5 \text{ cm}^{-1}$,⁴⁵ $519.6 \pm 0.8 \text{ cm}^{-1}$,⁴⁶ $519 \pm 1 \text{ cm}^{-1}$,⁴⁸ and $520.0 \pm 0.5 \text{ cm}^{-1}$.⁵⁴ These values can be compared with our measured period T_{ph} via $\bar{\nu} = 1/(cT_{ph})$. Converting our two experimental values of T_{ph} (the time-domain-analyzed value of $64.07 \pm 0.07 \text{ fs}$ and frequency-domain-analyzed value of $64.16 \pm 0.05 \text{ fs}$) yields center frequencies of $520.6 \pm 0.6 \text{ cm}^{-1}$ and $519.9 \pm 0.4 \text{ cm}^{-1}$, respectively. Satisfyingly, aside from the original Raman-

scattering measurement of the Si optic phonon by Russell,⁴⁴ these two results are consistent with the Raman-scattering values listed above.

V. SUMMARY

We have presented experimental data on the coherent excitation of the Si optic phonon with fs optical pulses at a photon energy of 1.55 eV. The results of these experiments have motivated an extension of the two-band TSRS model of Merlin *et al.* to include the finite lifetime of charge density that couples to the coherent oscillation. This extension formally combines the DECP and TSRS models of the force that drives the coherent phonon. We have discussed our experimental results from Si in terms of this combined model and shown that virtual excitations are primarily responsible for the nonzero phase. Using this model we have suggested a natural explanation of the nonzero phase of the E_g mode in Sb and have discussed prior results from Si and Ge. Our combined model should be generally applicable to describing the phase of coherent oscillations in cases where two-band terms dominate the Raman scattering. Further, it should be easily testable in other materials because all of the parameters involved in the model are directly obtainable from the ultrafast measurements that excite and probe the coherent vibrations and from frequency-dependent measurements of the dielectric function.

ACKNOWLEDGMENT

D.M.R. acknowledges useful discussions with R. Merlin.

APPENDIX A

Here we calculate the long-time solution to Eq. (1) with the initial conditions $Q(t \rightarrow -\infty) = 0$ and $\dot{Q}(t \rightarrow -\infty) = 0$, assuming that the force $F(t)$ lasts for only a finite time. From this solution we then obtain a general expression for the phase ϕ of the coherent oscillations in terms of the driving force $F(t)$.

The solution to Eq. (1) can be found in the manner used by Landau and Lifshitz to find the general solution of the undamped ($\beta = 0$) oscillator.⁵⁸ By introducing the variable

$$\xi = \frac{dQ}{dt} + (\beta + i\Omega_1)Q, \quad (\text{A1})$$

where $\Omega_1 = \sqrt{\Omega_0^2 - \beta^2}$, Eq. (1) can be rewritten as

$$\frac{d\xi}{dt} - (i\Omega_1 - \beta)\xi = F(t), \quad (\text{A2})$$

thus transforming the harmonic oscillator equation to a first-order equation. With the given initial conditions Eq. (A2) has the solution

$$\xi(t) = \exp[(i\Omega_1 - \beta)t] \int_{-\infty}^t dt' F(t') \exp[-(i\Omega_1 - \beta)t']. \quad (\text{A3})$$

The coherent amplitude Q is trivially determined from ξ by noting that Eq. (A1) implies $Q = \text{Im}(\xi)/\Omega_1$. In order to find

the phase of the oscillations we consider Eq. (A3) in the long-time limit, which is defined as anytime after the force $F(t)$ has vanished. In this limit the upper limit on the integral in Eq. (A3) can be replaced by ∞ .⁵⁹ Thus we may write (where LT indicates this long-time limit)

$$Q_{LT}(t) = \frac{1}{\Omega_1} \text{Im} \left\{ \exp[(i\Omega_1 - \beta)t] \int_{-\infty}^{\infty} dt' F(t') \times \exp[-(i\Omega_1 - \beta)t'] \right\}. \quad (\text{A4})$$

If we define the Fourier transform of a time-dependent function $f(t)$ as

$$\hat{f}(\Omega) = \frac{1}{\sqrt{2\pi}} \int_{-\infty}^{\infty} dt f(t) \exp(i\Omega t), \quad (\text{A5})$$

then Eq. (A4) can be expressed as

$$Q_{LT}(t) = \sqrt{\frac{\pi-i}{2\Omega_1}} \exp(-\beta t) [\exp(i\Omega_1 t) \hat{F}(-\Omega_1 - i\beta) - \exp(-i\Omega_1 t) \hat{F}^*(-\Omega_1 - i\beta)]. \quad (\text{A6})$$

This last equation can be rewritten as

$$Q_{LT}(t) = -\sqrt{2\pi} \sqrt{\xi_1^2 + \xi_2^2} \exp(-\beta t) \cos[\Omega_1 t + \arctan(\xi_2/\xi_1)], \quad (\text{A7})$$

where $\xi_1 = \text{Re}[i\hat{F}(-\Omega_1 - i\beta)]$ and $\xi_2 = \text{Im}[i\hat{F}(-\Omega_1 - i\beta)]$. Thus, the phase of the oscillations can be succinctly expressed as

$$\phi = \arctan \left\{ \frac{\text{Im}[i\hat{F}(-\Omega_1 - i\beta)]}{\text{Re}[i\hat{F}(-\Omega_1 - i\beta)]} \right\}. \quad (\text{A8})$$

APPENDIX B

Here we derive Eq. (15), our extension of the TSRS model of $\hat{F}(\Omega)$ to finite values of γ . In what follows we utilize the notation of Merlin and co-workers^{3,4} as much as possible. Using Eq. (A5) and ignoring the electric-field spatial dependence and polarization dependence [which only affects the absolute value of $F(t)$], we can write Eq. (6) of Ref. 3 as

$$F(t) = -\frac{1}{4\pi} \int_{-\infty}^{\infty} d\omega_1 \int_{-\infty}^{\infty} d\omega_2 \hat{E}_0^*(\omega_1) \times \exp(i\omega_1 t) R(\omega_1, \omega_2) \hat{E}_0(\omega_2) \exp(-i\omega_2 t), \quad (\text{B1})$$

where $\hat{E}_0(\omega)$ is the Fourier transform of the laser-pulse electric field $E_0(t)$ and $R(\omega_1, \omega_2)$ (discussed in detail below) is the Raman tensor that couples the radiation field to the coherently excited phonon. With a change of integration variables in Eq. (B1) to $\omega = \omega_1$, $d\omega = d\omega_1$ and $\Omega = \omega_2 - \omega_1$, $d\Omega = d\omega_2$, Eq. (B1) becomes

$$F(t) = -\frac{1}{4\pi} \int_{-\infty}^{\infty} d\Omega \int_{-\infty}^{\infty} d\omega \hat{E}_0^*(\omega) R(\omega, \omega + \Omega) \times \hat{E}_0(\omega + \Omega) \exp(-i\Omega t), \quad (\text{B2})$$

and a comparison of this equation with the inverse of Eq. (A5) allows ready identification of $\hat{F}(\Omega)$ as

$$\hat{F}(\Omega) = -\sqrt{\frac{1}{8\pi}} \int_{-\infty}^{\infty} d\omega \hat{E}_0^*(\omega) R(\omega, \omega + \Omega) \hat{E}_0(\omega + \Omega). \quad (\text{B3})$$

For values of Ω smaller than the spectral width of the laser pulse the product $\hat{E}_0^*(\omega) \hat{E}_0(\omega + \Omega)$ is sharply peaked at $\omega = \omega_0 - \Omega/2$ and $\omega = -\omega_0 - \Omega/2$, where ω_0 is the laser-pulse center frequency. If $R(\omega, \omega + \Omega)$ varies slowly near these frequencies, then we may approximately write

$$\hat{F}(\Omega) = -\sqrt{\frac{1}{8\pi}} \left[R(\omega_0 - \frac{1}{2}\Omega, \omega_0 + \frac{1}{2}\Omega) + R(-\omega_0 - \frac{1}{2}\Omega, -\omega_0 + \frac{1}{2}\Omega) \right] \times \int_{-\infty}^{\infty} d\omega \hat{E}_0^*(\omega) \hat{E}_0(\omega + \Omega). \quad (\text{B4})$$

Because $I(t) = c_1 |E_0(t)|^2$, where c_1 is a constant, we can express the integral in Eq. (B4) as $(\sqrt{2\pi}/c_1) \hat{I}(\Omega)$. The Fourier transform of the driving force $F(t)$ can thus be written as

$$\hat{F}(\Omega) = -\frac{1}{4c_1} \left[R(\omega_0 - \frac{1}{2}\Omega, \omega_0 + \frac{1}{2}\Omega) + R(-\omega_0 - \frac{1}{2}\Omega, -\omega_0 + \frac{1}{2}\Omega) \right] \hat{I}(\Omega). \quad (\text{B5})$$

We now consider the Raman tensor $R(\omega_1, \omega_2)$, which can be written as

$$R(\omega_1, \omega_2) = \left(\frac{e}{m\hbar} \right)^2 \frac{1}{V\omega_1\omega_2} [r(\omega_1, \omega_2) + r(-\omega_2, -\omega_1)], \quad (\text{B6})$$

where the function $r(\omega_1, \omega_2)$ is composed of three sums.³ Following Merlin and co-workers,^{3,4} we only consider the doubly resonant sum, expecting its contribution to dominate the other sums. With this approximation $r(\omega_1, \omega_2)$ is given by

$$r(\omega_1, \omega_2) = \sum_{m,n} \frac{\Pi_{0m}(\mathbf{k}_1) \Xi_{mn} \Pi_{n0}(\mathbf{k}_2)}{(\omega_m + i\gamma/2 - \omega_1)(\omega_n - i\gamma/2 - \omega_2)}. \quad (\text{B7})$$

Here $\Pi_{ij}(\mathbf{k})$ is the matrix element for transitions between electronic states i and j (with energies $\hbar\omega_i$ and $\hbar\omega_j$) induced by the radiation field with wave vector \mathbf{k} , while the electron-phonon matrix element Ξ_{ij} couples the states i and j with the concomitant creation (or destruction) of a phonon.^{38,39} The physical process represented by the summand in Eq. (B7) can be described as follows. A photon with wave vector \mathbf{k}_2 and frequency ω_2 induces an electronic transition from the ground state to the state n . This state then scatters to state m

with the creation of a phonon. The electronic system then makes a transition back to the ground state from the state m , emitting a photon with wave vector \mathbf{k}_1 and frequency ω_1 . Energy conservation requires the phonon frequency to be $\omega_2 - \omega_1$. The parameter γ is the excited-state decay rate, which is assumed to be the same for all states.

The sum in Eq. (B7) consists of two types of terms, known as two-band and three-band terms. In two-band scattering the two intermediate electronic states in each term are identical, so that $\omega_m = \omega_n$.³⁹ In the three-band terms either the excited electron or hole is in a different band in the two intermediate states (in the independent-electron approximation).^{38,39} We again follow Merlin and co-workers and only consider the two-band processes in Eq. (B7).⁴ (For Si the neglect of the three-band terms is not expected to be significant, at least for laser frequencies near or below the E_1 and $E_1 + \Delta_1$ gaps, because the dominant three-band terms, which involve the two valence bands associated with these two gaps, have the same spectral shape as the two bands terms.⁴¹) Rewriting Eq. (B7) (with the photon wave-vector dependence suppressed) as

$$r(\omega_1, \omega_2) = \sum_{m,n} \frac{\Pi_{0m} \Xi_{mn} \Pi_{n0}}{\omega_m - \omega_n + i\gamma + \omega_2 - \omega_1} \left(\frac{1}{\omega_n - i\gamma/2 - \omega_2} - \frac{1}{\omega_m + i\gamma/2 - \omega_1} \right), \quad (\text{B8})$$

we see that in the two-band approximation

$$r(\omega_1, \omega_2) = \frac{1}{\omega_2 - \omega_1 + i\gamma} \sum_m \Xi_m \left(\frac{1}{\omega_m - i\gamma/2 - \omega_2} - \frac{1}{\omega_m + i\gamma/2 - \omega_1} \right), \quad (\text{B9})$$

where, for brevity, we have written $\Pi_{0m} \Xi_{mn} \Pi_{n0}$ as Ξ_m . Substituting Eq. (B9) into Eq. (B6) and omitting terms with non-

resonant denominators, the terms in brackets in Eq. (B5) become

$$R\left(\omega_0 - \frac{1}{2}\Omega, \omega_0 + \frac{1}{2}\Omega\right) + R\left(-\omega_0 - \frac{1}{2}\Omega, -\omega_0 + \frac{1}{2}\Omega\right) = \left(\frac{e}{m\hbar}\right)^2 \frac{1}{V\Omega + i\gamma} \sum_m \frac{\Xi_m}{\omega_0^2 - \Omega^2/4} \left[\frac{1}{\omega_m - i\gamma/2 - (\omega_0 + \Omega/2)} - \frac{1}{\omega_m + i\gamma/2 - (\omega_0 - \Omega/2)} \right]. \quad (\text{B10})$$

A comparison of Eq. (B10) with the quantum-mechanical expression for the frequency-dependent dielectric function $\hat{\epsilon}$ (due to direct interband transitions)³⁷ shows that if all matrix elements are constant and $\omega_0^2 - \Omega^2/4$ is replaced by ω_m^2 (which is valid for each term as long as γ and Ω are much less than ω_m), then

$$R\left(\omega_0 - \frac{1}{2}\Omega, \omega_0 + \frac{1}{2}\Omega\right) + R\left(-\omega_0 - \frac{1}{2}\Omega, -\omega_0 + \frac{1}{2}\Omega\right) \approx \frac{c_2}{\Omega + i\gamma} \left[\hat{\epsilon}\left(\omega_0 + \frac{1}{2}\Omega\right) - \hat{\epsilon}^*\left(\omega_0 - \frac{1}{2}\Omega\right) \right], \quad (\text{B11})$$

where c_2 is a constant. Because $\Omega \ll \omega_0$, we can rewrite Eq. (B11) as

$$R\left(\omega_0 - \frac{1}{2}\Omega, \omega_0 + \frac{1}{2}\Omega\right) + R\left(-\omega_0 - \frac{1}{2}\Omega, -\omega_0 + \frac{1}{2}\Omega\right) \approx c_2 \frac{\Omega}{\Omega + i\gamma} \left[\epsilon_1'(\omega_0) + \frac{2\epsilon_2(\omega_0)}{-i\Omega} \right]. \quad (\text{B12})$$

Substituting Eq. (B12) into Eq. (B5) we finally have

$$\hat{F}(\Omega) = -\frac{c_2}{4c_1} \frac{\Omega}{\Omega + i\gamma} \left[\epsilon_1'(\omega_0) + \frac{2\epsilon_2(\omega_0)}{-i\Omega} \right] \hat{I}(\Omega). \quad (\text{B13})$$

We remark that in order for the $\hat{\epsilon}'_1 \rightarrow 0$ limit of the extended TSRS model to reduce to the DECP model, we must interpret the parameter γ in Eq. (B7) as the decay rate of the coupled charge density, which is introduced in Eq. (5). Note also that in the $\gamma \rightarrow 0$ limit Eq. (B13) becomes Eq. (10) of Ref. 4.

*Present address: Physics Department, Colorado School of Mines, Golden, CO 80401.

¹T. K. Cheng *et al.*, Appl. Phys. Lett. **57**, 1004 (1990); T. K. Cheng *et al.*, *ibid.* **59**, 1923 (1991); M. F. DeCamp, D. A. Reis, P. H. Bucksbaum, and R. Merlin, Phys. Rev. B **64**, 092301 (2001); M. Hase *et al.*, Appl. Phys. Lett. **69**, 2474 (1996); M. Hase, K. Ishioka, M. Kitajima, K. Ushida, and S. Hishita, *ibid.* **76**, 1258 (2000); M. Hase, M. Kitajima, S. I. Nakashima, and K. Mizoguchi, Phys. Rev. Lett. **88**, 067401 (2002); O. V. Misochko, M. Hase, K. Ishioka, and M. Kitajima, *ibid.* **92**, 197401 (2004); É. D. Murray, D. M. Fritz, J. K. Wahlstrand, S. Fahy, and D. A. Reis, Phys. Rev. B **72**, 060301(R) (2005); T. Dekorsy, H. Auer, C. Waschke, H. J. Bakker, H. G. Roskos, H. Kurz, V. Wagner, and P. Grosse, Phys. Rev. Lett. **74**, 738 (1995); S. Hunsche, K. Wienecke, T. Dekorsy, and H. Kurz, *ibid.* **75**, 1815 (1995).

²H. J. Zeiger, J. Vidal, T. K. Cheng, E. P. Ippen, G. Dresselhaus, and M. S. Dresselhaus, Phys. Rev. B **45**, 768 (1992).

³G. A. Garrett, T. F. Albrecht, J. F. Whitaker, and R. Merlin, Phys. Rev. Lett. **77**, 3661 (1996).

⁴T. E. Stevens, J. Kuhl, and R. Merlin, Phys. Rev. B **65**, 144304 (2002).

⁵M. Hase, K. Mizoguchi, H. Harima, S. I. Nakashima, and K. Sakai, Phys. Rev. B **58**, 5448 (1998).

⁶O. V. Misochko, K. Sakai, and S. I. Nakashima, Phys. Rev. B **61**, 11225 (2000).

⁷O. V. Misochko, M. Hase, and M. Kitajima, J. Phys.: Condens. Matter **16**, 1879 (2004).

⁸O. V. Misochko, M. Hase, and M. Kitajima, Phys. Solid State **46**, 1741 (2004).

⁹A. I. Lobad and A. J. Taylor, Phys. Rev. B **64**, 180301(R) (2001).

¹⁰S. Hunsche and H. Kurz, Appl. Phys. A: Mater. Sci. Process. **65**, 221 (1997).

¹¹M. Hase, K. Ishioka, J. Demsar, K. Ushida, and M. Kitajima, Phys. Rev. B **71**, 184301 (2005).

¹²J. M. Chwalek *et al.*, Appl. Phys. Lett. **57**, 1696 (1990); J. M. Chwalek, C. Uher, J. F. Whitaker, G. A. Mourou, and J. Agostinelli, *ibid.* **58**, 980 (1991); W. Albrecht, T. Kruse, and H. Kurz, Phys. Rev. Lett. **69**, 1451 (1992); O. V. Misochko *et al.*, Physica C **320**, 213 (1999); O. V. Misochko, K. Sakai, and S. I. Na-

- kashima, *ibid.* **329**, 12 (2000); O. V. Misochko, Phys. Lett. A **269**, 97 (2000); O. V. Misochko, Phys. Solid State **42**, 1204 (2000); O. V. Misochko and M. V. Lebedev, *ibid.* **43**, 1195 (2001); I. Bozovic, M. Schneider, Y. Xu, R. Sobolewski, Y. H. Ren, G. Lupke, J. Demsar, A. J. Taylor, and M. Onellion, Phys. Rev. B **69**, 132503 (2004).
- ¹³W. Kütt, W. Albrecht, and H. Kurz, IEEE J. Quantum Electron. **28**, 2434 (1992).
- ¹⁴G. C. Cho, W. Kütt, and H. Kurz, Phys. Rev. Lett. **65**, 764 (1990); W. Kütt, G. C. Cho, T. Pfeifer, and H. Kurz, Semicond. Sci. Technol. **7**, B77 (1992); T. Dekorsy, H. Kurz, X. Q. Zhou, and K. Ploog, Appl. Phys. Lett. **63**, 2899 (1993); T. Dekorsy, T. Pfeifer, W. Kütt, and H. Kurz, Phys. Rev. B **47**, 3842 (1993); G. C. Cho, H. J. Bakker, T. Dekorsy, and H. Kurz, *ibid.* **53**, 6904 (1996); Y. M. Chang, L. Xu, and H. W. K. Tom, Phys. Rev. Lett. **78**, 4649 (1997); T. Nakajima, H. Harima, and K. Sakai, J. Lumin. **76-77**, 6 (1998); O. V. Misochko, JETP **92**, 246 (2001).
- ¹⁵T. Pfeifer, T. Dekorsy, W. Kütt, and H. Kurz, Appl. Phys. A: Solids Surf. **55**, 482 (1992).
- ¹⁶T. Mishina, K. Nitta, and Y. Masumoto, Phys. Rev. B **62**, 2908 (2000); K. Ishioka, M. Hase, M. Kitajima, and K. Ushida, Appl. Phys. Lett. **78**, 3965 (2001).
- ¹⁷T. Pfeifer, W. Kütt, H. Kurz, and R. Scholz, Phys. Rev. Lett. **69**, 3248 (1992).
- ¹⁸R. Scholz, T. Pfeifer, and H. Kurz, Phys. Rev. B **47**, 16229 (1993).
- ¹⁹M. Hase, M. Kitajima, A. M. Constantinescu, and H. Petek, Nature (London) **426**, 51 (2003).
- ²⁰R. Scholz and A. Stahl, Phys. Status Solidi B **168**, 123 (1991); A. V. Kuznetsov and C. J. Stanton, Phys. Rev. Lett. **73**, 3243 (1994); Phys. Rev. B **51**, 7555 (1995); Á. R. Vasconcellos, R. Luzzi, and J. R. Madureira, J. Phys.: Condens. Matter **12**, 5325 (2000); A. V. Kuznetsov and C. J. Stanton, in *Ultrafast Phenomena in Semiconductors*, edited by K.-T. Tsen (Springer-Verlag, New York, 2001), p. 353; M. E. Garcia, T. Dumitrica, and H. O. Jeschke, Appl. Phys. A: Mater. Sci. Process. **79**, 855 (2004).
- ²¹R. Merlin, Solid State Commun. **102**, 207 (1997).
- ²²A. V. Bragas, C. Aku-Leh, S. Costantino, A. Ingale, J. Zhao, and R. Merlin, Phys. Rev. B **69**, 205306 (2004).
- ²³A. J. Sabbah and D. M. Riffe, Phys. Rev. B **66**, 165217 (2002).
- ²⁴D. M. Riffe and A. J. Sabbah, Rev. Sci. Instrum. **69**, 3099 (1998).
- ²⁵A. J. Sabbah and D. M. Riffe, J. Appl. Phys. **88**, 6954 (2000).
- ²⁶By convention, isotropic refers to that part of the distribution that has the same symmetry as the lattice, while anisotropic refers to that part of the distribution with P_2 (second-order Legendre polynomial) symmetry. Other lower-symmetry components can also exist. A detailed technical discussion can be found in J. L. Oudar, A. Migus, D. Hulin, G. Grillon, J. Etchepare, and A. Antonetti, Phys. Rev. Lett. **53**, 384 (1984).
- ²⁷B. S. Wherrett, A. L. Smirl, and T. F. Boggess, IEEE J. Quantum Electron. **19**, 680 (1983).
- ²⁸We use the convention that the phase ϕ is defined via $\cos(\omega t + \phi)$. When discussing phases reported in the literature we have converted, when necessary, those phases to this convention.
- ²⁹The results of these fits are insensitive to the low-frequency cutoff of the high-pass filter as long as the cutoff is less than $\sim 70\%$ of the optic-phonon frequency.
- ³⁰Although the phase ϕ is also a parameter in this analysis, its fitted value has no meaning because these filtered data have an arbitrary starting time of ~ 80 fs.
- ³¹Before calculating the Fourier transform, Eq. (3) must be windowed so as to match the length of a Fourier transformed data set. This is necessary because part of the width of the peak in the Fourier transform is due to truncation of the reflectivity data at $\Delta t = 7$ ps.
- ³²S. Tutihasi, G. G. Roberts, R. C. Keezer, and R. E. Drews, Phys. Rev. **177**, 1143 (1969).
- ³³P. Y. Wang and A. L. Jain, Phys. Rev. B **2**, 2978 (1970).
- ³⁴J. B. Renucci, W. Richter, M. Cardona, and E. Schönherr, Phys. Status Solidi B **60**, 299 (1973).
- ³⁵M. Cardona and D. L. Greenaway, Phys. Rev. **133**, A1685 (1964).
- ³⁶D. E. Aspnes and A. A. Studna, Phys. Rev. B **27**, 985 (1983).
- ³⁷C. C. Kim, J. W. Garland, H. Abad, and P. M. Raccah, Phys. Rev. B **45**, 11749 (1992).
- ³⁸R. Loudon, Proc. R. Soc. London, Ser. A **275**, 218 (1963).
- ³⁹A. K. Ganguly and J. L. Birman, Phys. Rev. **162**, 806 (1967).
- ⁴⁰G. Grosso and G. P. Parravicini, *Solid State Physics* (Academic Press, New York, 2000).
- ⁴¹J. B. Renucci, R. N. Tyte, and M. Cardona, Phys. Rev. B **11**, 3885 (1975).
- ⁴²G. E. Jellison, D. H. Lowndes, and R. F. Wood, Phys. Rev. B **28**, 3272 (1983); A. Compaan and H. J. Trodahl, *ibid.* **29**, 793 (1984).
- ⁴³P. C. Becker, H. L. Fragnito, C. H. Brito Cruz, R. L. Fork, J. E. Cunningham, J. E. Henry, and C. V. Shank, Phys. Rev. Lett. **61**, 1647 (1988).
- ⁴⁴J. P. Russell, Appl. Phys. Lett. **6**, 223 (1965).
- ⁴⁵J. H. Parker, Jr., D. W. Feldman, and M. Ashkin, Phys. Rev. **155**, 712 (1967).
- ⁴⁶T. R. Hart, R. L. Aggarwal, and B. Lax, Phys. Rev. B **1**, 638 (1970).
- ⁴⁷F. Cerdeira and M. Cardona, Phys. Rev. B **5**, 1440 (1972).
- ⁴⁸P. A. Temple and C. E. Hathaway, Phys. Rev. B **7**, 3685 (1973).
- ⁴⁹F. Cerdeira, T. A. Fjeldy, and M. Cardona, Solid State Commun. **8**, 133 (1970).
- ⁵⁰F. Cerdeira, T. A. Fjeldy, and M. Cardona, Phys. Rev. B **8**, 4734 (1973).
- ⁵¹F. Cerdeira, T. A. Fjeldy, and M. Cardona, Phys. Rev. B **9**, 4344 (1974).
- ⁵²K. Arya, M. A. Kanehisa, M. Jouanne, K. P. Jain, and M. Balkanski, J. Phys. C **12**, 3843 (1979).
- ⁵³M. Chandrasekhar, H. R. Chandrasekhar, M. Grimsditch, and M. Cardona, Phys. Rev. B **22**, 4825 (1980).
- ⁵⁴Z. Iqbal and Veprek, J. Phys. C **15**, 377 (1982).
- ⁵⁵J. Menéndez and M. Cardona, Phys. Rev. B **29**, 2051 (1984).
- ⁵⁶M. Balkanski, R. F. Wallis, and E. Haro, Phys. Rev. B **28**, 1928 (1983); A. Debernardi, S. Baroni, and E. Molinari, Phys. Rev. Lett. **75**, 1819 (1995); E. Haro-Poniatowski, J. L. Escamilla-Reyes, and K. H. Wanser, Phys. Rev. B **53**, 12121 (1996).
- ⁵⁷M. Balkanski, K. P. Jain, R. Beserman, and M. Jouanne, Phys. Rev. B **12**, 4328 (1975).
- ⁵⁸L. D. Landau and E. M. Lifshitz, *Mechanics* (Pergamon, New York, 1976).
- ⁵⁹The upper limit in the integral cannot be replaced by ∞ if $F(t)$ decays more slowly than $\exp(-\beta t)$, which is the case if $\gamma < \beta$. However, it can be shown that the solution derived here for the phase is valid even in this case.